MNRAS **000**, 1–13 (2016) Preprint 18 January 2016 Compiled using MNRAS LATEX style file v3.0

Supernovae and their host galaxies – III. The impact of bars and bulges on the radial distribution of supernovae in disc galaxies

A. A. Hakobyan,[1⋆] A. G. Karapetyan,[1] L. V. Barkhudaryan,[1] G. A. Mamon,[2] D. Kunth,[2] A. R. Petrosian,[1] V. Adibekyan,[3] L. S. Aramyan[1] and M. Turatto[4]

[1]*Byurakan Astrophysical Observatory, 0213 Byurakan, Aragatsotn province, Armenia*
[2]*Institut d'Astrophysique de Paris (UMR 7095: CNRS & UPMC), 98 bis Bd Arago, F-75014 Paris, France*
[3]*Centro de Astrofísica da Universidade do Porto, Rua das Estrelas, P-4150-762 Porto, Portugal*
[4]*INAF – Osservatorio Astronomico di Padova, Vicolo dell'Osservatorio 5, I-35122 Padova, Italy*

arXiv:1511.08896v2 [astro-ph.GA] 15 Jan 2016

Accepted 2015 December 2. Received 2015 November 28; in original form 2015 October 16

ABSTRACT

We present an analysis of the impact of bars and bulges on the radial distributions of the different types of supernovae (SNe) in the stellar discs of host galaxies with various morphologies. We use a well-defined sample of 500 nearby ($\leqslant 100$ Mpc) SNe and their low-inclined ($i \leqslant 60°$) and morphologically non-disturbed S0–Sm host galaxies from the Sloan Digital Sky Survey. We find that in Sa–Sm galaxies, all core-collapse (CC) and vast majority of SNe Ia belong to the disc, rather than the bulge component. The radial distribution of SNe Ia in S0–S0/a galaxies is inconsistent with their distribution in Sa–Sm hosts, which is probably due to the contribution of the outer bulge SNe Ia in S0–S0/a galaxies. In Sa–Sbc galaxies, the radial distribution of CC SNe in barred hosts is inconsistent with that in unbarred ones, while the distributions of SNe Ia are not significantly different. At the same time, the radial distributions of both types of SNe in Sc–Sm galaxies are not affected by bars. We propose that the additional mechanism shaping the distributions of Type Ia and CC SNe can be explained within the framework of substantial suppression of massive star formation in the radial range swept by strong bars, particularly in early-type spirals. The radial distribution of CC SNe in unbarred Sa–Sbc galaxies is more centrally peaked and inconsistent with that in unbarred Sc–Sm hosts, while the distribution of SNe Ia in unbarred galaxies is not affected by host morphology. These results can be explained by the distinct distributions of massive stars in the discs of early- and late-type spirals.

Key words: supernovae: general – galaxies: spiral – galaxies: stellar content – galaxies: structure.

1 INTRODUCTION

In the realm of disc galaxies, bars are a common feature observed in approximately 40 per cent of nearby S0–Sm galaxies (e.g. de Lapparent, Baillard & Bertin 2011). In the central regions of these disc galaxies, about one-third have strong barred structure, which generally affects both the motions of stars and interstellar gas and can affect spiral arms as well (for a comprehensive review see Kormendy & Kennicutt 2004). In addition, the relative sizes of bars and bulges seems to be correlated (e.g. Gadotti 2009), thus indicating that the growth of bars and bulges are somehow connected.

In spiral galaxies, most of the massive star formation occurs in the discs where bars, if present, have a strong impact on the radial distribution of star formation, particularly in early Hubble types. James, Bretherton & Knapen (2009) used Hα and R-band imaging to determine the distributions of young and old stellar populations in several hundreds of nearby S0/a–Im field galaxies. They identified a clear effect of bars on the pattern of massive star formation as a function of radius within discs. This effect results in a strongly enhanced Hα emission, and moderately enhanced R-band emission in both the central regions and at the bar-end radius of galaxies (see also James & Percival 2015). The authors noted that this effect seems to be stronger in galaxies classified as barred Sb or Sbc, where the overall distributions of star formation markedly different from that in their unbarred counterparts.

In this context, we are investigating the possible impact of stellar bars and bulges on the radial distributions of the different types of supernovae (SNe) in S0–Sm host galaxies. SNe are generally divided into two categories according to their progenitors: core-collapse (CC) and Type Ia SNe. CC SNe result from massive young stars that undergo CC (e.g. Turatto 2003; Smartt 2009;

⋆ E-mail: hakobyan@bao.sci.am

© 2016 The Authors

Anderson et al. 2012),[1] while Type Ia SNe are the end point in the evolution of binary stars when an older white dwarf (WD) accretes material from its companion, causing the WD mass to exceed the Chandrasekhar limit, or a double WD system loses angular momentum due to gravitational wave emission, leading to coalescence and explosion (for a comprehensive review, including the scenarios where the WD explodes at masses both above and below the Chandrasekhar limit, see Maoz, Mannucci & Nelemans 2014). The distribution of Type Ia SNe traces the distribution of R-band continuum emission/stellar mass in host disc galaxies, while the distribution of CC SNe is strongly related to the distribution of Hα emission/star formation (for the most recent review, see Anderson et al. 2015a). Therefore, it is expected that the above mentioned bar effect and a possible contribution from the old bulge populations in disc galaxies would leave their 'fingerprints' on the radial distributions of Type Ia and CC SNe.

In our earlier study (Hakobyan et al. 2009, hereafter H09), we attempted to find differences in the radial distributions of SNe in barred and unbarred spiral host galaxies (see also Petrosian et al. 2005; Hakobyan 2008; Nazaryan et al. 2013). No significant differences were found, most probably due to small number statistics, inhomogeneous data sets of SNe and their hosts, and unsatisfying considerations for the relations between the bar lengths, bulge sizes, and morphological types of SNe host galaxies. On the other hand, Wang, Höflich & Wheeler (1997) attempted to estimate the contribution from bulge components of spiral host galaxies to the entire radial distribution of SNe Ia. They noted that the stellar bulges in spirals are not efficient producers of Type Ia SNe (see also Anderson et al. 2015b). But again, the above mentioned impact of bars on the radial distributions of young and old stellar populations in the discs was not considered.

The aim of this article is to address these questions properly through a study of the radial distributions of Type Ia and CC (Ibc and II) SNe in a well-defined and homogeneous sample of 500 nearby SNe and their low-inclined and morphologically non-disturbed S0–Sm galaxies from the coverage of Sloan Digital Sky Survey-III (SDSS-III; Ahn et al. 2014).

In our first paper of this series (Hakobyan et al. 2012, hereafter Paper I), we have created a large and well-defined data base that combines extensive new measurements and a literature search of 3876 SNe and their 3679 host galaxies located within the sky area covered by the SDSS Data Release 8 (DR8). This data base is much larger than previous ones, and provides a homogeneous set of global parameters of SN hosts, including morphological classifications and measures of activity classes of nuclei. Moreover, in Paper I, we analysed and discussed many selection effects and biases, which usually affect the statistical studies of SNe. In the second article of the series Hakobyan et al. (2014, hereafter Paper II), we presented an analysis of the relative frequencies of the different SN types in nearby spiral galaxies with various morphological types and with or without bars. We used a subsample of spiral host galaxies of 692 SNe in different stages of galaxy–galaxy interaction and activity classes of nucleus. We proposed that the underlying mechanisms shaping the number ratios of SNe types could be interpreted within the framework of interaction-induced star formation, in addition to the known relations between morphologies and stellar populations. For more details, the reader is referred to Papers I and II.

This is the third paper of the series and the outline is as follows. Section 2 introduces sample selection and reduction. In Section 3, we give the results and discuss all the statistical relations. Our conclusions are summarized in Section 4. Throughout this paper, we adopt a cosmological model with $\Omega_{\rm m} = 0.27$, $\Omega_\Lambda = 0.73$, and a Hubble constant is taken as $H_0 = 73\,{\rm km\,s^{-1}\,Mpc^{-1}}$ (Spergel et al. 2007), both to conform to values used in our data base.

2 SAMPLE SELECTION AND REDUCTION

In this study, we compiled our sample by cross-matching the coordinates of classified Ia, Ibc[2], and II SNe from the Asiago Supernova Catalogue[3] (ASC; Barbon et al. 1999) with the coverage of SDSS DR10 (Ahn et al. 2014). All SNe are required to have coordinates and/or positions (offsets) with respect to the nuclei of their host galaxies. We use SDSS DR10 and the techniques presented in Paper I to identify the SNe host galaxies and classify their morphological types. Since we are interested in studying the radial distribution of SNe in stellar discs of galaxies, the morphologies of hosts are restricted to S0–Sm types.

In Paper I, we have shown that the sample of SNe is largely incomplete beyond $100\,{\rm Mpc}$ (see also Paper II). Thus, to avoid biasing the current sample against or in favour of one of the SN types, we truncate the sample to distances $\leqslant 100\,{\rm Mpc}$.

In addition, following the approach described in detail in Paper II, we classify the morphological disturbances of the host galaxies from the visible signs of galaxy–galaxy interactions in the SDSS DR10. We adopted the following categories for SN host disturbances: normal (hosts without any visible disturbance in their morphological structure), perturbed (hosts with visible morphological disturbance, but without long tidal arms, bridges, or destructed spiral patterns), interacting (hosts with obvious signs of galaxy–galaxy interaction), merging (hosts with ongoing merging process), and post-merging/remnant (single galaxies that exhibit signs of a past interaction, with a strong or relaxed disturbance). Here, we make use of this classification in order to exclude from the present analysis any host galaxy exhibiting strong disturbances (interacting, merging, and post-merging/remnant).

We measure the geometry of host galaxies using the Graphical Astronomy and Image Analysis[4] (GAIA) tool according to the approaches presented in Paper I.[5] First, we construct $25\,{\rm mag\,arcsec^{-2}}$ isophotes in the SDSS DR10 g-band, and then we visually fit on to each isophote an elliptical aperture centred at

[1] CC SNe are observationally classified in three major classes, according to the strength of lines in optical spectra (e.g. Filippenko 1997): Type II SNe show hydrogen lines in their spectra, including the IIn (dominated by emission lines with narrow components) and IIb (transitional objects with observed properties closer to SNe II at early times, then metamorphosing to SNe Ib) subclasses; Type Ib SNe show helium but not hydrogen, while Type Ic SNe show neither hydrogen nor helium. All these SNe types arise from young massive progenitors with possible differences in their masses, metallicities, ages, and fractions of binary stellar systems (e.g. Smith et al. 2011).

[2] By SN Ibc, we denote stripped-envelope SNe of Types Ib and Ic, as well as mixed Ib/c whose specific subclassification is uncertain.

[3] We use the updated version of the ASC to include all classified SNe exploded before 2014 January 1.

[4] GAIA is available for download as part of JAC Starlink Release at `http://starlink.jach.hawaii.edu`.

[5] The data base of Paper I is based on the SDSS DR8. Here, because we added new SNe in the sample, for homogeneity we re/measure the geometry of all host galaxies based only on DR10.

Table 1. Numbers of SNe at distances $\leqslant 100$ Mpc and inclinations $i \leqslant 60^\circ$ within host disc galaxies as a function of morphological types, split between barred and unbarred.

	Barred											
	S0	S0/a	Sa	Sab	Sb	Sbc	Sc	Scd	Sd	Sdm	Sm	All
Ia	1	9	5	8	13	13	13	6	12	3	0	83
Ib	0	0	0	0	1	5	3	0	1	2	1	13
Ib/c	0	0	0	0	0	2	0	0	0	0	0	2
Ic	0	0	0	0	1	3	5	4	4	0	0	17
II	0	0	0	2	15	17	19	8	25	8	2	96
IIb	0	0	1	0	0	3	2	0	2	0	0	8
All	1	9	6	10	30	43	42	18	44	13	3	219
	Unbarred											
	S0	S0/a	Sa	Sab	Sb	Sbc	Sc	Scd	Sd	Sdm	Sm	All
Ia	7	11	4	4	10	22	26	5	4	0	4	97
Ib	0	0	0	1	0	7	8	2	0	0	0	18
Ib/c	0	0	0	1	3	0	1	1	1	0	0	7
Ic	0	0	0	0	1	6	13	2	1	0	0	23
II	1	0	0	0	15	22	64	13	6	3	2	126
IIb	0	0	0	0	0	0	5	3	0	2	0	10
All	8	11	4	6	29	57	117	26	12	5	6	281

Among the SNe types, there are only 31 uncertain (':' or '*') and 35 peculiar ('pec') classifications. All Type IIn SNe are removed from the sample due to uncertainties in their progenitor nature, and often in their classification (e.g. Anderson et al. 2012; Habergham et al. 2014).

each galaxy centroid position. From the fitted elliptical apertures, we derive the major axes (D_{25}), elongations (a/b), and position angles (PA) of the major axes of galaxies. In further analysis, we use the D_{25} corrected for Galactic and host galaxy internal extinction. We then calculate the inclinations of host galaxies using elongations and morphological types following the classical Hubble formula. More details on these procedures are found in Paper I. Finally, an additional restriction on the inclinations ($i \leqslant 60^\circ$) of hosts is required to minimize absorption and projection effects in the discs of galaxies.[6]

After these restrictions, we are left with a sample of 500 SNe within 419 host galaxies.[7] For these host galaxies, we do visual inspection of the combined SDSS g-, r-, and i-band images, as well as check the different bands separately to detect any sign of barred structure in the stellar discs. In Paper I, we demonstrated that given their superior angular resolution and three-colour representations, the SDSS images, especially for low-inclined galaxies, offer a much more reliable and capacious source for bar detection than do the other images, e.g. plate-based images on which most of the HyperLeda/NED classifications were performed. To check the consistency of bar detection in our sample with that of the SDSS-based EFIGI[8] catalogue of nearby visually classified 4458 PGC galaxies (Baillard et al. 2011), we select a subsample of 149 galaxies that are common to both EFIGI and to our sample of SNe hosts. Following Paper II, we compare the EFIGI `Bar Length` attribute[9] with our detection (bar or no bar). When the `Bar Length` is 0 or 2, our bar detection is different for only 6 per cent of cases. When the `Bar Length` is 3 or 4, our bar detection completely matches with that of the EFIGI. However, we do not detect bars in 30 per cent of the cases when `Bar Length` is 1. Hence, the EFIGI `Bar Length` $= 1$ mainly corresponds to the threshold of our bar detection, i.e., barely visible bar feature with a length about one-tenth of D_{25}.[10] Table 1 displays the distribution of all SNe types among the various considered morphological types for their barred and unbarred host galaxies.

3 RESULTS AND DISCUSSION

We now study the possible influence of bars and bulges on the SNe distributions through an analysis of the radial distributions of different types of SNe in discs of host galaxies with various morphological types. Here, we widely use our morphological classification, bar detection, and geometry for SNe host galaxies, while for bulge parameters (e.g. bulge-to-disc mass ratio: B/D) we only indirectly consider their statistical relations to the Hubble sequence (e.g. de Lapparent et al. 2011).

3.1 Galactocentric radius deprojection and normalization

We apply the inclination correction to the projected (observed) galactocentric radii of SNe as described in H09. The reliability of the inclination correction is based on the fundamental assumption that SNe belong mostly to the disc, rather than the bulge component in S0–Sm galaxies (e.g. Johnson & MacLeod 1963; McCarthy 1973; Barbon et al. 1975; Iye & Kodaira 1975; Vettolani & Zamorani 1977; Tsvetkov 1981, 1987; Kazarian 1997; Ivanov et al. 2000; Wang et al. 2013). This assumption is natural for CC SNe, considering the requirement that massive young stars are progenitors (e.g. Smartt 2009; Anderson et al. 2012) located in the discs of host galaxies (e.g. Onic et al. 2008; H09). The spatial distribution of SNe Ia, arising from older WD in binary systems (e.g. Maoz et al. 2014), is more complicated and consists of two interpenetrating components (e.g. Hatano, Branch & Deaton 1998): disc and bulge SNe.

If SNe belong mostly to the bulge component, one would expect that the distributions of their projected galactocentric distances (normalized to the g-band $25^{\rm th}$ magnitude isophotal semimajor axis; $R_{25} = D_{25}/2$) along major (U/R_{25}) and minor (V/R_{25}) axes would be the same both in face-on ($i \leqslant 60^\circ$) and in edge-on ($i > 60^\circ$) disc galaxies. The projected U and V galactocentric distances (in arcsec) of an SN are

$$\begin{aligned} U &= \Delta\alpha \sin {\rm PA} + \Delta\delta \cos {\rm PA} \, , \\ V &= \Delta\alpha \cos {\rm PA} - \Delta\delta \sin {\rm PA} \, , \end{aligned} \qquad (1)$$

where $\Delta\alpha$ and $\Delta\delta$ are offsets of the SN in equatorial coordinate

[6] The sample with $i > 60^\circ$ is only used in Section 3.1 for ancillary purposes.
[7] The full data base of 500 individual SNe (SN designation, type, and offset from host galaxy nucleus) and their 419 host galaxies (galaxy SDSS designation, distance, morphological type, bar, corrected g-band D_{25}, a/b, PA, and inclination) is available in the online version of this article.
[8] Extraction de Formes Idéalisées de Galaxies en Imagerie.
[9] This attribute quantifies the presence of a central bar component in the galaxy, in terms of length relative to the galaxy major axis D_{25}. `Bar Length` $= 0$ (no visible bar); 1 (barely visible bar feature); 2 (short bar, with a length about one-third of D_{25}); 3 (long bar, that extends over about half of D_{25}); 4 (very long, prominent bar that extends over more than half of D_{25}).
[10] Later in the study, we will see that this very central region of galaxies with tiny bars is almost always restricted to the first bin of the radial distribution of SNe, and therefore cannot statistically bias our results.

system, and PA is position angle of the major axis of the host galaxy. For more details of these formulae, the reader is referred to H09.

The R_{25} normalization is important because the distribution of linear distances (in kpc) is strongly biased by the greatly different intrinsic sizes of host galaxies (see fig. 2 in H09). In linear scale, there would be a systematic overpopulation of SNe at small galactocentric distances as this region would be populated by SNe exploding in all host galaxies, including the smaller ones, while larger distances would only be populated by the SNe occurring in the larger hosts.

Fig. 1 shows (in red) the V/R_{25} versus U/R_{25} distributions in face-on and edge-on S0–Sm galaxies, as well as their histograms. The sample of SNe in face-on galaxies consists of 180 Ia and 320 CC SNe (see Table 1), while the ancillary sample of SNe in edge-on hosts (not shown in Table 1) includes 105 Ia and 181 CC SNe. In disc galaxies, all types of SNe preferentially appear along the major U axis (see the standard deviations in Table 2). This effect is stronger in edge-on galaxies. In fact, the two-sample Kolmogorov–Smirnov (KS) and Anderson–Darling (AD) tests,[11] shown in Table 2, indicate that the distributions of U/R_{25} and V/R_{25} are significantly different, both for Type Ia and CC SNe (except for Type Ia SNe in face-on hosts with the KS test).

It is worth mentioning that Sa–Sm galaxies contain stellar populations of different ages and host both Type Ia and CC SNe. While S0 and S0/a galaxies, which are mostly populated by old stars and have prominent bulges, host Type Ia SNe. A tiny fraction of CC SNe has also been detected in galaxies classified as S0. Nevertheless, in these rare cases, there is some evidence of residual star formation in the SN hosts, due to merging/accretion or interaction with close neighbours in the past (e.g. Hakobyan et al. 2008; Paper I). The distribution of SNe types versus morphology of the host galaxies, shown in Table 1, is consistent with this picture. In this sense, when selecting only Sa–Sm hosts, the $P_{\rm KS}$ for Type Ia SNe in the face-on sample becomes significant (it is reduced to 0.045), suggestive of a possible contribution from bulge SNe Ia in S0–S0/a galaxies. For Sa–Sm galaxies, the probabilities of KS and AD tests for the other subsamples do not change the results of Table 2.

Performing simple calculations, we find that the ratio of the mean values of $|V|$ and $|U|$ is 0.71 for Type Ia and 0.75 for CC SNe in face-on, and, respectively, 0.35 and 0.36 in edge-on galaxies. These numbers are very close to the mean values of the cosines of the inclinations ($\langle\cos\ i\rangle = 0.74 \pm 0.01$ in face-on galaxies and 0.31 ± 0.02 in edge-on galaxies – where the uncertainties are the errors on the means), thus supporting the fact that the vast majority of SNe in S0–Sm galaxies are distributed within the stellar discs. Similar results are found when only considering Sa–Sm galaxies. This also suggests that the rate of SNe Ia in spiral galaxies is dominated by a relatively young/intermediate progenitor population (e.g. Mannucci et al. 2005; Hakobyan et al. 2011; Li et al. 2011).

For deprojected host discs, in Fig. 1 we also show (in black) the V/r_{25} versus U/R_{25} distributions and their histograms for different samples, where r_{25} is the g-band 25th magnitude isophotal semiminor axis ($r_{25} = R_{25}\ \cos\ i$). In contrast to the previous normalization, the KS and AD tests show that the distributions of U/R_{25} and V/r_{25} both for Type Ia and CC SNe could be drawn from the same parent distribution (see Table 2). In addition, the ratios of the mean values of $|V|/r_{25}$ and $|U|/R_{25}$ in different samples are approximately equal to unity. Thus, after correcting the host galaxies for inclination effects, the distributions of SNe along major (U/R_{25}) and minor (V/r_{25}) axes turn to be equivalent (see also the standard deviations in Table 2). Hereafter, we restrict our analysis to the face-on sample to minimize absorption and projection effects in the discs of galaxies.[12]

We now adopt the oversimplified model where all SNe are distributed on infinitely thin discs of the host galaxies. While this is a reasonable assumption for SNe within spiral hosts, we shall extend this assumption to S0–S0/a galaxies, for which many find a disc distribution of SNe (e.g. Onic et al. 2008; H09 for CC and Hamuy & Pinto 1999; Ivanov et al. 2000 for Type Ia SNe).

In this thin-disc approximation, the corrected galactocentric radius (in arcsec) of the SN in the host disc satisfies

$$R_{\rm SN}^2 = U^2 + \left(\frac{V}{\cos\,i}\right)^2 . \qquad (2)$$

We pay particular attention and discuss the cases when the contribution from the bulge SNe Ia becomes apparent, especially in S0–S0/a hosts.

3.2 Influence of bars and bulges on the radial distribution of SNe

The upper panel of Fig. 2 compares the distributions of deprojected, normalized galactocentric radii ($\tilde{r} = R_{\rm SN}/R_{25}$) of Type Ia and CC SNe in S0–S0/a and Sa–Sm galaxies. In this panel, we see an initial rise of SNe number as a function of $\tilde{r}$ and a negative radial gradient outside the maximum, suggestive of the exponential surface brightness distribution of stellar discs, which we will study in more detail in Section 3.3. In previous studies, based on smaller samples, similar deprojected distributions of SNe were already obtained by normalizing them to the radii of hosts at some fixed surface brightness isophot (Johnson & MacLeod 1963; Barbon et al. 1975; Iye & Kodaira 1975; Vettolani & Zamorani 1977; Bartunov & Tsvetkov 1986; Turatto et al. 1989; Petrosian & Turatto 1990, 1995; Li & Li 1995; Ivanov et al. 2000; Navasardyan et al. 2001; Bressan et al. 2002; Petrosian et al. 2005; Hakobyan 2008; Anderson & James 2009; H09; Wang et al. 2010; Nazaryan et al. 2013; Wang et al. 2013).

The observed numbers of SNe at $\tilde{r} \lesssim 0.2$ indicate that different SN searches fail to discover objects at or near the centre of the surveyed galaxies (e.g. Cappellaro et al. 1997; Hamuy & Pinto 1999). In an earlier study, Shaw (1979) noted that this effect is stronger for distant host galaxies relative to nearer ones. Then it became apparent that this *Shaw effect* is important for deep photographic searches and negligible for visual and CCD searches (e.g. Cappellaro et al. 1997; Howell et al. 2000). Presently, SN searches are conducted only with CCD cameras and SNe are discovered via image subtraction, so the discrimination against SNe occurring near the bright nuclei of galaxies is less strong. Nevertheless, an area with a radius of a few pixels centred on every galaxy nucleus is usually excluded during a search, because galactic nuclei often suffer imperfect image subtraction and introduce many false sources (e.g. Leaman et al. 2011). Another difficulty is that extinction by

[11] The two-sample AD test is more powerful than the KS test (Engmann & Cousineau 2011), being more sensitive to differences in the tails of distributions. Traditionally, we chose the threshold of 5 per cent for significance levels of the different tests.

[12] The edge-on galaxies will be the sample for our forthcoming paper with a different method of analysis.

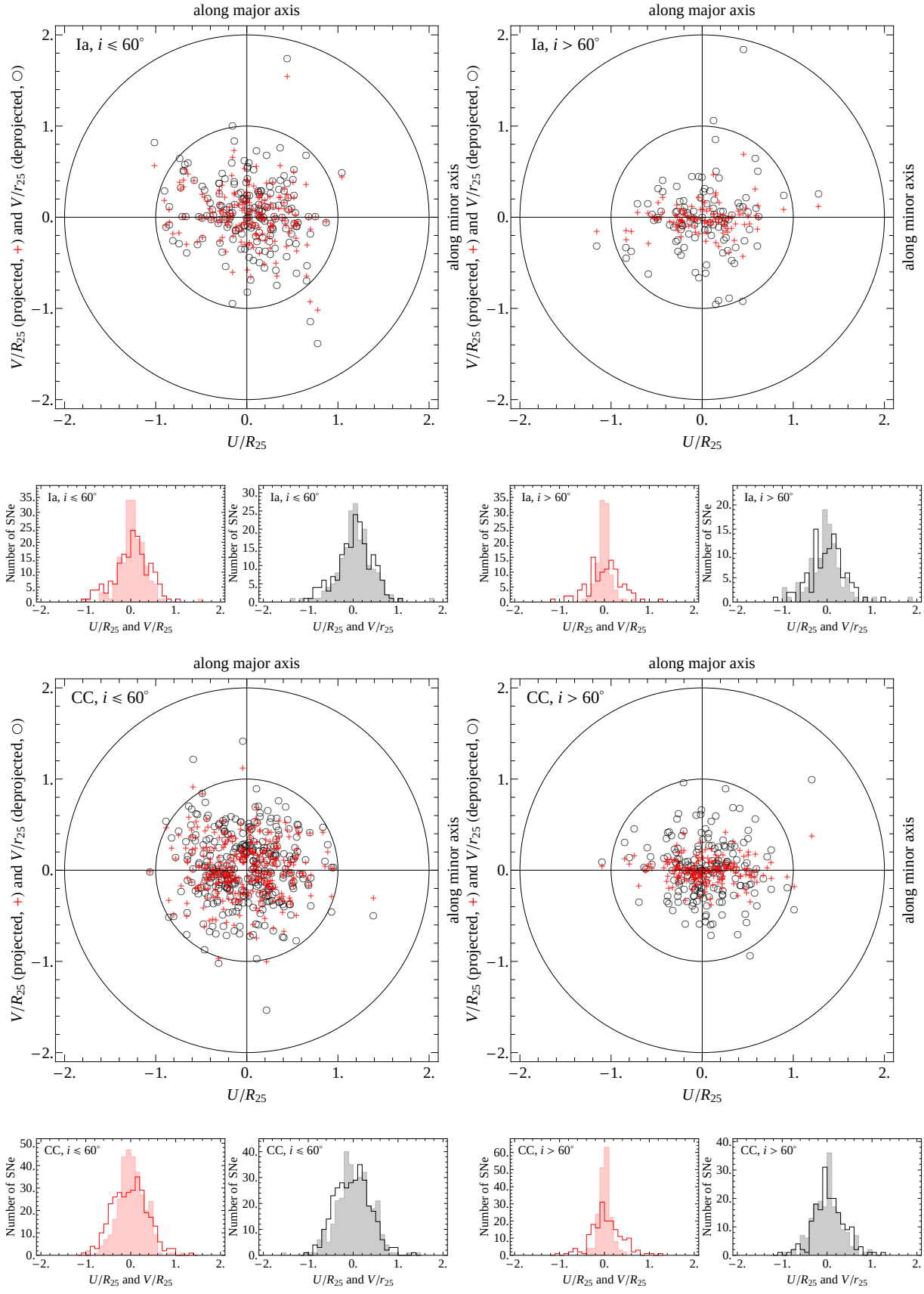

Figure 1. Distributions of normalized galactocentric distances of Type Ia and CC SNe along major (U/R_{25}) and minor (V/R_{25} and V/r_{25}) axes in face-on ($i \leqslant 60^\circ$) and edge-on ($i > 60^\circ$) disc (S0–Sm) galaxies, where $r_{25} = R_{25} \cos i$ is the isophotal semiminor axis. The red crosses represent U/R_{25} and V/R_{25} pairs, while the black open circles show U/R_{25} and V/r_{25} pairs. The solid histograms are the distributions of U/R_{25}, while the shaded histograms are the distributions of V/R_{25} and V/r_{25}. The two concentric circles are the host galaxy R_{25} and $2R_{25}$ sizes.

Table 2. Comparison of the 2D spatial distributions of SNe among different subsamples of S0–Sm galaxies.

Subsamples (1) versus (2)	SN	$i \leqslant 60^\circ$					$i > 60^\circ$				
		$N_{\rm SN}$	σ_1	σ_2	$P_{\rm KS}$	$P_{\rm AD}$	$N_{\rm SN}$	σ_1	σ_2	$P_{\rm KS}$	$P_{\rm AD}$
U/R_{25} versus V/R_{25}	Ia	180	0.394	0.299	0.217	**0.026**	105	0.385	0.154	**0.001**	**0.000**
U/R_{25} versus V/R_{25}	CC	320	0.382	0.299	**0.003**	**0.002**	181	0.349	0.132	**0.000**	**0.000**
U/R_{25} versus V/r_{25}	Ia	180	0.394	0.387	0.561	0.646	105	0.385	0.390	0.174	0.321
U/R_{25} versus V/r_{25}	CC	320	0.382	0.384	0.120	0.162	181	0.349	0.327	0.564	0.568

The $P_{\rm KS}$ and $P_{\rm AD}$ are the probabilities from two-sample KS and AD tests, respectively, that the two distributions being compared (with respective standard deviations σ_1 and σ_2) are drawn from the same parent distribution. The $P_{\rm KS}$ and $P_{\rm AD}$ are calculated using the calibrations by Massey (1951) and Pettitt (1976), respectively. The statistically significant differences between the distributions are highlighted in bold.

dust in host galaxy discs, depending on inclination, can affect the radial distributions of SNe, particularly in the nuclear region (e.g. Wang et al. 1997; Hatano et al. 1998; Holwerda et al. 2015).

To check the possible influences of these selection effects on the radial distribution of SNe, we compare, in Table 3, the radial distributions of SNe in different pairs of subsamples where these selection effects may produce different radial SN distributions. For this, we performed two-sample KS and AD tests between the pairs of radial SN distributions. These tests show that the radial distributions of Type Ia and CC SNe in our sample are not affected by distance or inclination of the host galaxy, nor by the SN discovery epoch (photographic/CCD searches).

We now compare, in Table 4, the distributions of the normalized deprojected radii for pairs of subsamples that should not be affected by selection effects. We see no statistically significant differences between the radial distributions of Type Ia and CC SNe in all the subsamples of Sa–Sm galaxies. In contrast, the cumulative radial distributions of SNe Ia in S0–S0/a and Sa–Sm galaxies apparently deviate from one another (as seen in the AD statistic but only very marginally so in the KS statistic). Fig. 2, indeed shows signs of a bimodal radial distribution for SNe Ia in S0–S0/a galaxies.

Naturally, one expects that among disc galaxies, bulge SNe Ia should have highest contribution to the whole distribution of SNe Ia in S0–S0/a subsample, because among disc galaxies the ratio of bulge luminosity over disc luminosity (or B/D) is highest in the S0–S0/a subsample (e.g. Yoshizawa & Wakamatsu 1975; Simien & de Vaucouleurs 1986; Oohama et al. 2009; de Lapparent et al. 2011). In the case of Sa–Sm galaxies, both Type Ia and CC SNe dominate in the Sbc–Sc morphological bin (see Table 1), where the B/D ratio is significantly lower than that in S0–S0/a galaxies (e.g. Oohama et al. 2009; de Lapparent et al. 2011). Moreover, the radial distributions of Type Ia and CC SNe in all the Sa–Sm subsamples can be drawn from the same parent distribution (see the P-values in Table 4) supporting the fact that in these galaxies SNe Ia mostly exploded in the disc component where all CC SNe also occur. Thus, the apparent deviation of the radial distribution of Type Ia SNe in S0–S0/a galaxies from that in Sa–Sm hosts (upper panel of Fig. 2) is attributed to the contribution by SNe Ia from the bulge component of S0–S0/a galaxies.

Another interesting results stands out in Table 4. The radial distributions of CC SNe in barred versus unbarred Sa–Sbc galaxies are inconsistent (middle panel of Fig. 2), while for Type Ia SNe the radial distributions between barred and unbarred Sa–Sbc galaxies are not significantly different. At the same time, the radial distributions of both Type Ia and CC SNe in Sc–Sm galaxies are not affected by bars.

Interestingly, James et al. (2009) discovered that several early-type barred spiral galaxies that had strong dips in their radial Hα line emission profiles, near $0.25\,R_{25}$.[13] This region is roughly where their unbarred counterparts host the strongest star formation. The Hα emission from barred Sb–Sbc galaxies showed central components and concentrations of star formation at or just outside the bar-end radius. Except for the central component, where we have difficulties to discover SNe, the picture of James et al. is very similar to that we observe for CC SNe in barred and unbarred Sa–Sbc galaxies (see the middle panel of Fig. 2 and fig. 8 in James et al.). The region between the central component and bar-end radius of Hα emission profiles is termed the 'star formation desert' (SFD) by James & Percival (2015). In addition, they noted that the SFD had significant continuum emission in the R-band and even showed line emission not consistent with expectations from star formation, but most probably from an old stellar population.

Taking into consideration that the distributions of Type Ia and CC SNe, respectively, trace the distributions of R-band continuum emission/stellar mass and Hα emission/star formation (e.g. James & Anderson 2006; Anderson & James 2009), we compare the inner ($\tilde{r} \leqslant 0.3$) fractions of different SNe ($F_{\rm SN}$) in barred and unbarred host galaxies (see Table 5). This inner region is selected because in Sa–Sbc subsample the SNe dominate in Sb–Sbc galaxies (see Table 1), where the mean SFD region has outer radius ~ 0.3 of the optical radius (see fig. 5 in James et al. 2009).[14]

Table 5 shows that the inner $\tilde{r} \leqslant 0.3$ fractions of Type Ia SNe in Sa–Sbc and Sc–Sm hosts are not statistically different between barred and unbarred galaxies. The same situation holds true for CC SNe in Sc–Sm galaxies. However, the inner fraction of CC SNe is significantly lower in barred Sa–Sbc galaxies compared with their unbarred counterparts. It is important to note that the inner fractions of Type Ia and CC SNe are not statistically different one from another when the same morphological and barred/unbarred categories are selected.

The results of Table 5 agree quite well with the findings of James & Percival (2015) that barred galaxies of earlier Hubble types have substantially suppressed star formation (see also

[13] The dip in Hα occurs at one-quarter of the isophotal radius corresponding to a surface magnitude of $\mu_R = 24\,{\rm mag\,arcsec^{-2}}$, which in turn is roughly equal to R_{25}.

[14] Ideally, instead of using the $\tilde{r} \leqslant 0.3$ region, we could perform bar length measurements for each of barred galaxy in the sample to obtain the fractions of different SNe in the radial range swept by bars. However, this is beyond the scope of this paper, and will be the subject of a future paper.

Table 3. Comparison of the normalized, deprojected radial distributions of SNe among different pairs of subsamples possibly affected by selection effects.

Subsample 1		Subsample 2	Ia				CC			
			$N_{\rm SN}(1)$	$N_{\rm SN}(2)$	$P_{\rm KS}$	$P_{\rm AD}$	$N_{\rm SN}(1)$	$N_{\rm SN}(2)$	$P_{\rm KS}$	$P_{\rm AD}$
$0 < D({\rm Mpc}) \leqslant 60$ (S0–S0/a)	versus	$60 < D({\rm Mpc}) \leqslant 100$ (S0–S0/a)	10	18	0.566	0.416	0	1	–	–
$0 < D({\rm Mpc}) \leqslant 60$ (Sa–Sm)	versus	$60 < D({\rm Mpc}) \leqslant 100$ (Sa–Sm)	69	83	0.692	0.620	168	151	0.683	0.465
$0^\circ \leqslant i \leqslant 40^\circ$ (S0–S0/a)	versus	$40^\circ < i \leqslant 60^\circ$ (S0–S0/a)	11	17	0.973	0.883	0	1	–	–
$0^\circ \leqslant i \leqslant 40^\circ$ (Sa–Sm)	versus	$40^\circ < i \leqslant 60^\circ$ (Sa–Sm)	64	88	0.190	0.412	134	185	0.938	0.821
$t \leqslant 2000\,{\rm yr}$ (S0–S0/a)	versus	$t > 2000\,{\rm yr}$ (S0–S0/a)	6	22	0.348	0.560	0	1	–	–
$t \leqslant 2000\,{\rm yr}$ (Sa–Sm)	versus	$t > 2000\,{\rm yr}$ (Sa–Sm)	58	94	0.997	0.857	108	211	0.517	0.635

Each pair of the subsamples is selected, if possible, to include comparable numbers of SNe in both subsamples.

Table 4. Comparison of the normalized, deprojected radial distributions of SNe among different pairs of subsamples.

Subsample 1				Subsample 2				
Host	SN	$N_{\rm SN}$		Host	SN	$N_{\rm SN}$	$P_{\rm KS}$	$P_{\rm AD}$
S0–S0/a	Ia	28	versus	Sa–Sm	Ia	152	0.099	**0.020**
Sa–Sm	Ia	152	versus	Sa–Sm	CC	319	0.568	0.259
Sa–Sm (barred)	Ia	73	versus	Sa–Sm (barred)	CC	136	0.483	0.378
Sa–Sm (unbarred)	Ia	79	versus	Sa–Sm (unbarred)	CC	183	0.349	0.342
Sa–Sm (barred)	Ia	73	versus	Sa–Sm (unbarred)	Ia	79	0.192	0.313
Sa–Sm (barred)	CC	136	versus	Sa–Sm (unbarred)	CC	183	0.060	0.076
Sa–Sbc	Ia	79	versus	Sa–Sbc	CC	106	0.683	0.751
Sa–Sbc (barred)	Ia	39	versus	Sa–Sbc (barred)	CC	50	0.528	0.627
Sa–Sbc (unbarred)	Ia	40	versus	Sa–Sbc (unbarred)	CC	56	0.702	0.473
Sa–Sbc (barred)	Ia	39	versus	Sa–Sbc (unbarred)	Ia	40	0.242	0.617
Sa–Sbc (barred)	CC	50	versus	Sa–Sbc (unbarred)	CC	56	**0.008**	**0.028**
Sc–Sm	Ia	73	versus	Sc–Sm	CC	213	0.424	0.276
Sc–Sm (barred)	Ia	34	versus	Sc–Sm (barred)	CC	86	0.670	0.575
Sc–Sm (unbarred)	Ia	39	versus	Sc–Sm (unbarred)	CC	127	0.340	0.355
Sc–Sm (barred)	Ia	34	versus	Sc–Sm (unbarred)	Ia	39	0.503	0.615
Sc–Sm (barred)	CC	86	versus	Sc–Sm (unbarred)	CC	127	0.581	0.276
Sa–Sbc	Ia	79	versus	Sc–Sm	Ia	73	0.850	0.956
Sa–Sbc	CC	106	versus	Sc–Sm	CC	213	0.183	0.156
Sa–Sbc (barred)	Ia	39	versus	Sc–Sm (barred)	Ia	34	0.992	0.967
Sa–Sbc (barred)	CC	50	versus	Sc–Sm (barred)	CC	86	0.489	0.278
Sa–Sbc (unbarred)	Ia	40	versus	Sc–Sm (unbarred)	Ia	39	0.822	0.961
Sa–Sbc (unbarred)	CC	56	versus	Sc–Sm (unbarred)	CC	127	**0.033**	0.067

The statistically significant differences between the distributions are highlighted in bold.

Table 5. Fractions of inner ($R_{\rm SN} \leqslant 0.3\,R_{25}$) SNe in barred and unbarred host galaxies.

Host	SN	Barred		Unbarred		$P_{\rm B}$
		$N_{\rm SN}$	$F_{\rm SN}$	$N_{\rm SN}$	$F_{\rm SN}$	
Sa–Sbc	Ia	39	$0.26^{+0.05}_{-0.04}$	40	$0.38^{+0.05}_{-0.05}$	0.170
Sa–Sbc	CC	50	$0.20^{+0.04}_{-0.03}$	56	$0.36^{+0.04}_{-0.04}$	**0.044**
Sc–Sm	Ia	34	$0.26^{+0.05}_{-0.05}$	39	$0.36^{+0.05}_{-0.05}$	0.240
Sc–Sm	CC	86	$0.26^{+0.03}_{-0.03}$	127	$0.28^{+0.02}_{-0.02}$	0.741

The standard deviations of the fractions are calculated using the approach of Cameron (2011). The significance value $P_{\rm B}$ is calculated using Barnard's exact test (Barnard 1945), which compares the pairs of numbers rather than the fractions. The statistically significant difference between the fractions is highlighted in bold.

James et al. 2009), hence the lack of CC SNe in the inner radial range swept by the strong bars of Sa–Sbc galaxies. On the other hand, this region is not 'forbidden' to Type Ia SNe, because these SNe originate from an older stellar population also located in the bulge. CC SNe in barred Sc–Sm galaxies can appear in the inner regions because the effect of star formation suppressing by bars is not seen in late-type barred galaxies (James et al. 2009; James & Percival 2015). Thus, we see that bars of host galaxies affect the radial distributions of SNe, at least the CC ones, in the stellar discs of early-type galaxies.

According to Table 4 and the bottom panel of Fig. 2, we also see that the radial distribution of CC SNe in unbarred Sa–Sbc galaxies is more centrally peaked and inconsistent with that in unbarred Sc–Sm hosts (as seen in the KS statistic but only marginally so in the AD statistic). In contrast, the radial distribution of Type Ia SNe in unbarred galaxies is unaffected by host morphology.

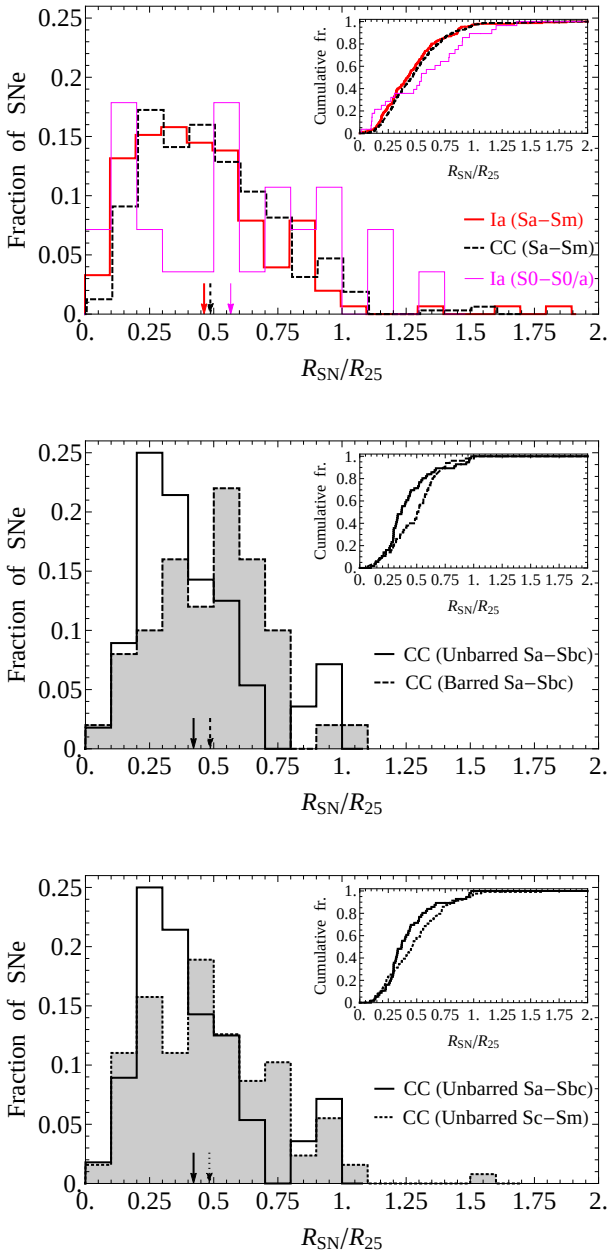

Figure 2. Upper panel: distributions of deprojected and normalized galactocentric radii ($\tilde{r} = R_{SN}/R_{25}$) of Type Ia SNe in S0–S0/a and Sa–Sm hosts, as well as CC SNe in Sa–Sm galaxies. Middle panel: the distributions of CC SNe in barred and unbarred Sa–Sbc hosts. Bottom panel: the distributions of CC SNe in unbarred Sa–Sbc and Sc–Sm galaxies. The insets present the cumulative distributions of SNe. The mean values of the distributions are shown by arrows.

The different radial distributions of SNe in unbarred spirals can be explained by the strong dependence of massive star formation distribution in the discs on the morphological type of galaxies. In particular, for S0/a–Im galaxies James et al. (2009) studied the distribution of Hα and R-band concentration indices (C30)[15] as a function of Hubble type. They found a strong correlation of Hα C30 index with Hubble sequence, with the early-type having about two times higher Hα C30 indices in comparison with the late-type galaxies. The same is true for R-band C30 indices, but with less difference between early- and late-type galaxies (see fig 1. in James et al. 2009). Moreover, the authors showed that the unbarred galaxies have more centrally concentrated Hα emission than do their strongly barred counterparts. Note that, in some cases, the C30 indices may be biased by Active Galactic Nuclei (AGN) emission from the very central region ($< 0.2R_{25}$) of galaxies. However, fig. 8 in James et al. (2009) shows that for unbarred early-type galaxies the trends above are virtually unaffected when the inner regions ($< 0.2R_{25}$) are not considered. Since Type Ia SNe are less tightly connected to the Hα emission of the explosion site (e.g. Stanishev et al. 2012; Galbany et al. 2014), the radial distribution of SNe Ia in Sa–Sm hosts is not strongly affected by the morphology.

It is important to note that, when selecting Sa–Sbc and Sc–Sm morphologies without splitting between barred and unbarred subsamples, all the significant differences in the radial distributions of SNe are washed out (see Table 4). Therefore, the lack of significant differences in the radial distributions of CC SNe as a function of the morphological type of host galaxies presented in the earlier studies (e.g. Bartunov et al. 1992; Li & Li 1995; Tsvetkov, Pavlyuk & Bartunov 2004; Petrosian et al. 2005; Hakobyan 2008; H09; Wang et al. 2010) is a consequence of these samples mixing barred and unbarred galaxies with different levels of mixing of the stellar populations.

To exclude the effects of (1) bars (two distinct types of bars: strong bars, which are more common in early-type discs, and weak bars, which are frequently found in late-type spirals; see fig. 5 of Paper II) and (2) the morphological differences between Type Ia and CC SNe hosts (the mean morphological type of SNe Ia host galaxies is earlier than that of the CC SNe hosts, as can be deduced from the numbers in our Table 1; see also fig. 2 and table 11 of Paper II), we repeat the analysis of the inner ($\tilde{r} \leqslant 0.3$) fractions of SNe, restricting to unbarred morphological bins (Sbc and Sb–Sbc). We carry out this analysis because the bulge stars of Sb–Sbc galaxies are typically located in our chosen inner region,[16] which enables a better estimation of the possible contribution of bulge SNe Ia on top of that of the inner disc population. We find that there is no significant difference in the inner fractions of Type Ia and CC SNe in the Sbc bin ($F_{\rm Ia} = 0.32^{+0.07}_{-0.06}$ and $F_{\rm CC} = 0.31^{+0.05}_{-0.05}$). Even selecting unbarred Sb–Sbc bins where the bulge should be (slightly) more prominent, we get $F_{\rm Ia} = 0.31^{+0.06}_{-0.05}$ and $F_{\rm CC} = 0.33^{+0.04}_{-0.04}$. Here, we do not use the earlier morphological bins because they are rarely populated by CC SNe making it impossible to estimate the $F_{\rm CC}$ (see Table 1). On the other hand, the later morphological bins are not suitable because of the weaker bulge component (e.g. Oohama et al. 2009; de Lapparent et al. 2011).

Interestingly, $F_{\rm Ia} = 0.32^{+0.06}_{-0.05}$ for 28 Type Ia SNe in all S0–S0/a galaxies, which is the same as $F_{\rm Ia} = 0.32^{+0.02}_{-0.02}$ for 152 SNe Ia in all Sa–Sm hosts and even the same as $F_{\rm Ia}$ for only unbarred Sbc galaxies. With the results in Section 3.1, this suggests that the deviation of the radial distribution of Type Ia SNe in S0–S0/a galaxies from that in Sa–Sm hosts (upper panel of Fig. 2 and Table 4) is

[15] The C30 index is the ratio of the flux within 0.3 times the optical radius and the total flux, which provides a simple measure of the observed radial distribution of the luminosity of a galaxy in a specified bandpass.

[16] Fig. 23 of Bernardi et al. (2014) indicates that the bulge half-light radius, $R_{\rm bulge}$, is roughly one-quarter of the disc scale length, which for typical central disc surface brightness amounts to $R_{\rm bulge} < R_{25}/10$ (using the relation between disc scale length and R_{25} given in equation 3 of H09).

mostly attributed to the contribution by the outer bulge SNe Ia in S0–S0/a galaxies (see also the corresponding mean values of $\tilde{r}$ in Fig. 2).

These results confirm that the old bulges of Sa–Sm galaxies are not significant producers of Type Ia SNe, while the bulge populations are significant for SNe Ia only in S0–S0/a galaxies. In S0–S0/a hosts, the relative fraction of bulge to disc SNe Ia is probably changed in comparison with that in Sa–Sm hosts, because the progenitor population from the discs of S0–S0/a galaxies should be much lower due to the lower number of young/intermediate stellar populations.

Moreover, we do not detect the relative deficiency of Type Ia SNe in comparison with CC SNe in the inner regions of spiral hosts, contrary to van den Bergh (1997), Wang et al. (1997), and Anderson et al. (2015b). Instead, the radial distributions of both types of SNe are well matched between each other in all the subsamples of Sa–Sbc and Sc–Sm galaxies supporting the idea that the relative concentration of CC SNe in the centres of spirals found by these authors is most probably due to a contribution of the central excess of CC SNe in disturbed galaxies (e.g. Habergham, James & Anderson 2012; Paper II), which are excluded from our sample (see Section 2).

Wang et al. (1997) discussed the possibilities that the relative deficiency of Type Ia SNe that they found (and which we do not confirm) in the inner regions of spiral galaxies may be due to a stronger dust extinction for Type Ia events than for CC SNe. They suggested that massive progenitors of CC SNe within associations might create large cavities in the discs through their own stellar winds or earlier SN explosions, therefore making the discovery of CC SNe easier. Despite the higher luminosity of Type Ia SNe at maximum, their lower mass progenitors make such cavities less likely (see also van den Bergh & McClure 1990). However, our results discussed above show that dust extinction in the discs of nearby non-disturbed spirals should not be different for Type Ia and CC SNe. Moreover, in Aramyan et al. (in preparation), we show that although CC SNe are more concentrated to the brightness peaks of spiral arms than are Type Ia events, both SN types occur mostly in spiral arms (see also Bartunov, Tsvetkov & Filimonova 1994; McMillan & Ciardullo 1996) where large cavities, if present, should be shared, on average, between the progenitors of both SN types.

The differences between our results and those of previous studies is that we deproject and normalize the galactocentric radii of SNe, while the other studies used projected and normalized (van den Bergh 1997), or projected linear (Wang et al. 1997), or normalized to flux (Anderson et al. 2015b) galactocentric radii. Another important difference is that, contrary to our study, Wang et al. (1997) and Anderson et al. (2015b) included highly inclined galaxies in their studies.

3.3 The deprojected exponential surface density distribution

It is widely accepted that the surface density distribution of SNe in discs follows an exponential law (e.g. Barbon et al. 1975; Vettolani & Zamorani 1977; Bartunov et al. 1992; van den Bergh 1997; H09; Wang et al. 2010; Nazaryan et al. 2013). However, a comprehensive analysis of the surface density distribution in different samples of barred and unbarred galaxies has not been performed and this is one of the main goals of the present study.

Following H09, we fit an exponential surface density profile, $\Sigma(R)$, to the distribution of deprojected normalized radii, using maximum likelihood estimation (MLE). Here, $\Sigma^{\rm SN}(\tilde{r}) = \Sigma_0^{\rm SN} \exp(-\tilde{r}/\tilde{h}_{\rm SN})$, where $\tilde{h}_{\rm SN}$ is the scale length of the distribution and $\Sigma_0^{\rm SN}$ is the central surface density of SNe. To check whether the distribution of SN radii follows the best-fitting exponential surface density profile, we perform one-sample KS and AD tests on the normalized cumulative distributions of SNe, where the exponential model has a cumulative normalized distribution $E(\tilde{r}) = 1 - (1 + \tilde{r}/\tilde{h}_{\rm SN}) \exp(-\tilde{r}/\tilde{h}_{\rm SN})$.

In columns 3–6 of Table 6, the total number of SNe in the full radial range, their mean radius with standard deviation, the KS and AD test P-values, $P_{\rm KS}$ and $P_{\rm AD}$ are, respectively, presented for the different subsamples. In Table 7, despite the small number statistics of Type Ibc SNe (see Table 1), we consider Types Ibc and II SNe separately.

From columns 5 and 6 of Tables 6 and 7, we see that in many subsamples of CC SNe, in contrast to Type Ia SNe, the surface density distribution is not consistent with an exponential profile. Fig. 2 hints that the observed inconsistency is probably due to the central $\tilde{r} \lesssim 0.2$ deficit of SNe (farther, see also in the right-hand panel of Fig. 3). For this reason, we repeat the above described tests for $\tilde{r} \in [0.2; \infty)$ range and find that the inconsistency vanishes in most of the subsamples (see columns 8 and 9 in Tables 6 and 7). The corresponding scale lengths for the inner-truncated disc are listed in column 10 of Tables 6 and 7. As expected, only the distribution of CC SNe in early-type barred spirals is inconsistent with an exponential distribution due to the impact of bars on the radial distribution of CC SNe as discussed in Section 3.2. The effect is not seen for Type Ibc SNe probably due to the small number statistics of these SNe in early-type barred spirals (see column 7 in Tables 7).

Finally, to eliminate the effects induced by bars, we compare the radial distributions of Types Ibc and II SNe in unbarred spiral galaxies only. The two-sample KS and AD tests show that the radial distribution of Type Ibc SNe is highly inconsistent with that of Type II ($P_{\rm KS} = 0.026$ and $P_{\rm AD} = 0.014$), because the former are more centrally concentrated (see the mean of $\tilde{r}$ and $\tilde{h}_{\rm SN}$ values in Table 7).

The radial position within host galaxies can be used as a proxy for the local metallicity since the short lifetime of CC SN progenitor (tens of Myr) is not enough to allow far migration from its birthplace. Therefore, the physical explanation for the more concentrated distribution of SNe Ibc with respect to SNe II in non-disturbed and unbarred spiral galaxies is that SNe Ibc arise from more metal-rich environments,[17] as has been widely discussed (e.g. van den Bergh 1997; Petrosian et al. 2005; Hakobyan 2008; Prieto, Stanek & Beacom 2008; Boissier & Prantzos 2009; Anderson & James 2009; H09; Anderson et al. 2012). Here, we do not go into deeper considerations, instead we refer the reader to the mentioned references for more complete discussions.

Despite the smaller numbers statistics, we analyse the radial distributions of Types Ib and Ic SNe in unbarred galaxies (18 SNe Ib and 23 SNe Ic; see Table 1). Compared with the SNe Ibc versus SNe II test, the radial distributions of SNe Ib and SNe Ic are sufficiently similar that the two-sample KS and AD tests fail to distinguish them with statistical significance ($P_{\rm KS} = 0.119$ and $P_{\rm AD} = 0.202$). In the inner-truncated disc, the scale length of Type Ib SNe (0.14 ± 0.03) is not significantly lower from that of Type

[17] The top-heavy initial mass function and/or enhanced close binary fraction in the central regions of strongly disturbed/interacting galaxies might play an important role in explaining the inner excess of SNe Ibc compared to SNe II (e.g. Habergham et al. 2012; Kangas et al. 2013; Anderson et al. 2015a). However, the roles of these factors are difficult to estimate, since our analysis is restricted to non-disturbed host galaxies.

Table 6. Consistency of CC and Type Ia SN distributions with an exponential surface density model.

		$\tilde{r} \in [0;\infty)$				$\tilde{r} \in [0.2;\infty)$			
Host	SN	$N_{\rm SN}$	$\langle\tilde{r}\rangle \pm \sigma$	$P_{\rm KS}$	$P_{\rm AD}$	$N_{\rm SN}$	$P_{\rm KS}$	$P_{\rm AD}$	$\tilde{h}_{\rm SN}$
(1)	(2)	(3)	(4)	(5)	(6)	(7)	(8)	(9)	(10)
S0–S0/a	Ia	28	0.57 ± 0.38	0.593	0.344	21	0.297	0.455	0.32 ± 0.04
Sa–Sm	Ia	152	0.46 ± 0.28	0.209	0.091	127	0.533	0.488	0.21 ± 0.02
Sa–Sm (barred)	Ia	73	0.47 ± 0.23	0.095	0.076	64	0.421	0.244	0.21 ± 0.03
Sa–Sm (unbarred)	Ia	79	0.46 ± 0.32	0.520	0.548	63	0.962	0.912	0.22 ± 0.02
Sa–Sbc	Ia	79	0.46 ± 0.29	0.441	0.295	69	0.968	0.980	0.21 ± 0.02
Sa–Sbc (barred)	Ia	39	0.46 ± 0.23	0.315	0.210	35	0.595	0.601	0.20 ± 0.03
Sa–Sbc (unbarred)	Ia	40	0.47 ± 0.34	0.864	0.874	34	0.683	0.917	0.21 ± 0.03
Sc–Sm	Ia	73	0.46 ± 0.27	0.443	0.265	58	0.432	0.408	0.22 ± 0.02
Sc–Sm (barred)	Ia	34	0.47 ± 0.24	0.279	0.359	29	0.424	0.477	0.22 ± 0.03
Sc–Sm (unbarred)	Ia	39	0.45 ± 0.30	0.666	0.628	29	0.932	0.792	0.23 ± 0.03
Sa–Sm	CC	319	0.49 ± 0.26	**0.001**	**0.000**	286	0.075	0.056	0.21 ± 0.01
Sa–Sm (barred)	CC	136	0.52 ± 0.26	**0.045**	**0.005**	125	0.062	0.116	0.23 ± 0.02
Sa–Sm (unbarred)	CC	183	0.46 ± 0.25	**0.028**	**0.008**	161	0.454	0.359	0.20 ± 0.01
Sa–Sbc	CC	106	0.45 ± 0.21	**0.004**	**0.008**	95	0.102	0.118	0.19 ± 0.02
Sa–Sbc (barred)	CC	50	0.49 ± 0.21	**0.050**	**0.029**	45	**0.030**	**0.046**	0.21 ± 0.04
Sa–Sbc (unbarred)	CC	56	0.42 ± 0.22	**0.035**	0.052	50	0.384	0.432	0.17 ± 0.03
Sc–Sm	CC	213	0.50 ± 0.27	**0.036**	**0.004**	191	0.125	0.190	0.23 ± 0.02
Sc–Sm (barred)	CC	86	0.54 ± 0.29	0.118	0.066	80	0.715	0.785	0.24 ± 0.03
Sc–Sm (unbarred)	CC	127	0.48 ± 0.26	0.146	**0.041**	111	0.164	0.226	0.22 ± 0.02

Columns 1 and 2 give the subsample; Col. 3 is the number of SNe in the subsample for the full radial range $\tilde{r} \in [0;\infty)$; Col. 4 is the mean of $\tilde{r}$ with standard deviation; Cols. 5 and 6 are the $P_{\rm KS}$ and $P_{\rm AD}$ probabilities from one-sample KS and AD tests, respectively, that the distribution of SNe is drawn from the best-fitting exponential surface density profile; Cols. 7, 8, and 9 are, respectively, the same as Cols. 3, 5, and 6, but for $\tilde{r} \in [0.2;\infty)$; Col. 10 is the maximum likelihood value of $\tilde{h}_{\rm SN} = h_{\rm SN}/R_{25}$ with bootstrapped error (repeated 10^4 times) for the inner-truncated disc. The $P_{\rm KS}$ and $P_{\rm AD}$ are calculated using the calibrations by Massey (1951) and D'Agostino & Stephens (1986), respectively. The statistically significant deviations from an exponential law are highlighted in bold.

Table 7. Consistency of Types Ibc and II SN distributions with an exponential surface density model.

		$\tilde{r} \in [0;\infty)$				$\tilde{r} \in [0.2;\infty)$			
Host	SN	$N_{\rm SN}$	$\langle\tilde{r}\rangle \pm \sigma$	$P_{\rm KS}$	$P_{\rm AD}$	$N_{\rm SN}$	$P_{\rm KS}$	$P_{\rm AD}$	$\tilde{h}_{\rm SN}$
(1)	(2)	(3)	(4)	(5)	(6)	(7)	(8)	(9)	(10)
Sa–Sm	Ibc	80	0.40 ± 0.20	0.063	**0.043**	67	0.240	0.396	0.17 ± 0.02
Sa–Sm (barred)	Ibc	32	0.42 ± 0.22	0.485	0.383	27	0.698	0.649	0.18 ± 0.02
Sa–Sm (unbarred)	Ibc	48	0.38 ± 0.19	0.121	0.105	40	0.430	0.713	0.16 ± 0.02
Sa–Sbc	Ibc	31	0.35 ± 0.15	0.112	0.093	25	0.127	0.160	0.14 ± 0.02
Sa–Sbc (barred)	Ibc	12	0.37 ± 0.18	0.308	0.536	9	0.204	0.251	0.17 ± 0.03
Sa–Sbc (unbarred)	Ibc	19	0.34 ± 0.12	0.170	0.114	16	0.419	0.482	0.13 ± 0.02
Sc–Sm	Ibc	49	0.43 ± 0.23	0.267	0.277	42	0.477	0.855	0.18 ± 0.03
Sc–Sm (barred)	Ibc	20	0.45 ± 0.24	0.670	0.591	18	0.792	0.984	0.19 ± 0.03
Sc–Sm (unbarred)	Ibc	29	0.41 ± 0.23	0.589	0.616	24	0.881	0.911	0.18 ± 0.03
Sa–Sm	II	239	0.52 ± 0.27	**0.005**	**0.000**	219	0.063	0.052	0.23 ± 0.01
Sa–Sm (barred)	II	104	0.55 ± 0.27	0.074	**0.007**	98	0.113	0.131	0.24 ± 0.02
Sa–Sm (unbarred)	II	135	0.49 ± 0.26	0.093	**0.024**	121	0.393	0.323	0.22 ± 0.02
Sa–Sbc	II	75	0.49 ± 0.23	**0.012**	**0.022**	70	0.323	0.220	0.21 ± 0.02
Sa–Sbc (barred)	II	38	0.52 ± 0.20	**0.029**	**0.029**	36	**0.022**	**0.050**	0.22 ± 0.03
Sa–Sbc (unbarred)	II	37	0.46 ± 0.25	0.097	0.229	34	0.588	0.668	0.19 ± 0.03
Sc–Sm	II	164	0.53 ± 0.28	0.079	**0.008**	149	0.189	0.155	0.24 ± 0.01
Sc–Sm (barred)	II	66	0.56 ± 0.30	0.176	0.107	62	0.571	0.711	0.25 ± 0.03
Sc–Sm (unbarred)	II	98	0.50 ± 0.27	0.140	0.051	87	0.186	0.197	0.23 ± 0.02

The explanation for the columns is the same as for Table 6. In the SNe II subsample, there are 18 Type IIb SNe (see Table 1) with $\langle\tilde{r}\rangle \pm \sigma = 0.61 \pm 0.25$, suggesting that in terms of the radial distribution they likely belong to SNe II rather than to SNe Ibc group. The statistically significant deviations from an exponential law are highlighted in bold.

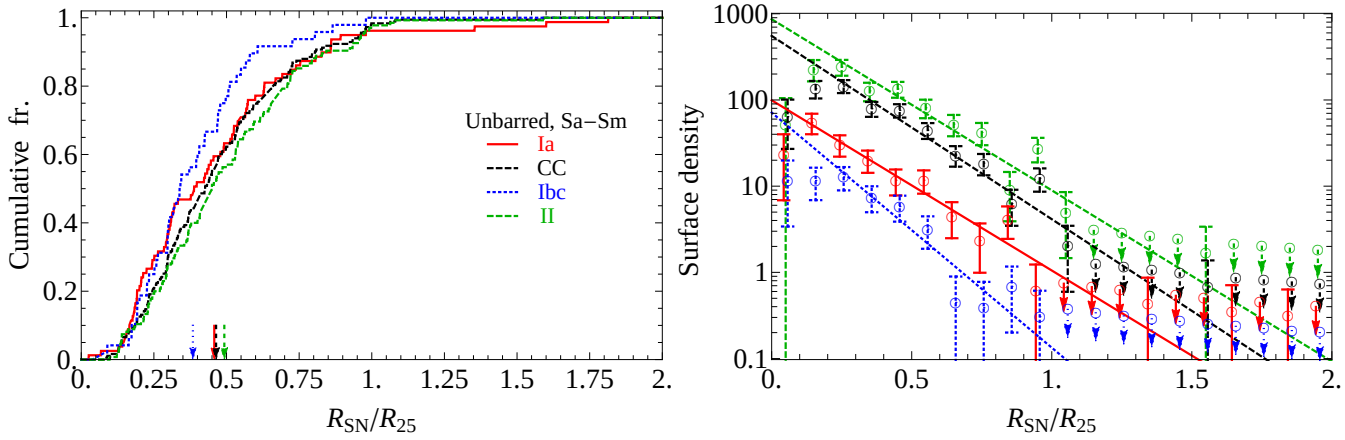

Figure 3. Left: cumulative fractions of the different types of SNe versus deprojected and normalized galactocentric radius ($\tilde{r} = R_{SN}/R_{25}$) in unbarred Sa–Sm host galaxies. The mean $\tilde{r}$ values of each SNe type are shown by arrows. Right: surface density distributions (with arbitrary normalization) of the different types of SNe in the same subsample of hosts. The different lines show the maximum likelihood exponential surface density profiles estimated for the inner-truncated disc. The error bars assume a Poisson distribution. Down arrows represent the upper-limits of surface density (with ± 1 SN if none is found). For better visibility, the distributions are shifted vertically sorted by increasing the mean $\tilde{r}$ as one moves upwards.

Ic SNe (0.17 ± 0.03), while the scale length of all the Ibc family is between these values (see Table 7).

Fig. 3 presents the cumulative and surface density distributions of the different types of SNe in unbarred Sa–Sm host galaxies. According to the scale lengths in Tables 6 and 7, the fit lines in Fig. 3 show the exponential surface density profiles of SNe in the same subsample. A central ($\tilde{r} \lesssim 0.2$) drop from an exponential distribution is observed for all the SNe types, less prominent for SNe Ia.

It is important to note that the scale lengths of SNe ($\tilde{h}_{SN} = h_{SN}/R_{25}$) in Tables 6 and 7 are calculated using the $\mu_g = 25\,\mathrm{mag\,arcsec^{-2}}$ isophotal level in the SDSS g-band (see Section 2), while the previous papers used the same magnitude isophotal level in B-band (e.g. Tsvetkov et al. 2004; H09; Wang et al. 2010; Herrero-Illana et al. 2012; Kangas et al. 2013). In Paper I, we showed that galaxies have sizes systematically larger in the g-band than in the B-band (see fig. 11 and table 4 in Paper I) due to the fact that our g-band measurements are performed at the equivalent of the $\langle \mu_B \rangle \simeq 25.48$ isophote, hence at typically lower surface brightness threshold. Therefore, considering that our radii of host galaxies are greater than those in the HyperLeda on average by a factor of 1.32 ± 0.01 (see Paper I), we get generally about 25 per cent smaller scale lengths of SNe in g-band compared with the earlier estimations in B-band (e.g. see H09 for CC SNe).

4 CONCLUSIONS

In this third paper of a series, using a well-defined and homogeneous sample of SNe and their host galaxies from the coverage of SDSS DR10, we analyse the impact of bars and bulges on the radial distributions of the different types of SNe in the stellar discs of host galaxies with various morphologies. Our sample consists of 419 nearby ($\leqslant 100$ Mpc), low-inclination ($i \leqslant 60^\circ$), and morphologically non-disturbed S0–Sm galaxies, hosting 500 SNe in total.

All the results that we summarize below concerning the radial distributions of SNe in barred galaxies can be explained considering the strong impact of the bars on the distribution of massive star formation in stellar discs of galaxies, particularly in early-type spirals. On the other hand, the bulge component of Type Ia SNe distribution shows a negligible impact on the radial distribution of SNe Ia, except in S0-S0/a galaxies.

We also check that there are no strong selection effects and biases within our SNe and host galaxies samples, which could drive the observed behaviours of the radial distributions of Type Ia and CC SNe in the disc galaxies presented in this study.

The results obtained in this article are summarized below, along with their interpretations.

(i) In Sa–Sm galaxies, all CC and the vast majority of Type Ia SNe belong to the disc, rather than the bulge component (Fig. 1 and Table 2). The result suggests that the rate of SNe Ia in spiral galaxies is dominated by a relatively young/intermediate progenitor population. This observational fact makes the deprojection of galactocentric radii of both types of SNe a key point in the statistical studies of their distributions.

(ii) The radial distribution of Type Ia SNe in S0–S0/a galaxies is inconsistent with that in Sa–Sm hosts (as seen in Fig. 2 and Table 4 for the AD statistic but only very marginally so in the KS statistic). This inconsistency is mostly attributed to the contribution by SNe Ia in the outer bulges of S0–S0/a galaxies. In these hosts, the relative fraction of bulge to disc SNe Ia is probably changed in comparison with that in Sa–Sm hosts, because the progenitor population from the discs of S0–S0/a galaxies should be much lower due to the lower number of young/intermediate stellar populations.

(iii) The radial distribution of CC SNe in barred Sa–Sbc galaxies is not consistent with that of unbarred Sa–Sbc hosts (Fig. 2 and Table 4), while for Type Ia SNe the distributions are not significantly different (Table 4). At the same time, the radial distributions of both Type Ia and CC SNe in Sc–Sm galaxies are not affected by bars (Table 4). These results are explained by a substantial suppression of massive star formation in the radial range swept by strong bars of early-type barred galaxies.

(iv) The radial distribution of CC SNe in unbarred Sa–Sbc galaxies is more centrally peaked and inconsistent with that in unbarred Sc–Sm hosts (as seen in Fig. 2 and Table 4 for the KS statistic but only marginally so in the AD statistic). On the other hand, the radial distribution of Type Ia SNe in unbarred galaxies is not

affected by host morphology (Table 4). These results can be well explained by the distinct distributions of massive stars in the discs of early- and late-type spirals. In unbarred Sa–Sbc galaxies, star formation is more concentrated to the inner regions (Hα emission outside the nucleus) and should thus be responsible for the observed radial distribution of CC SNe.

(v) The radial distribution of CC SNe, in contrast to Type Ia SNe, is inconsistent with the exponential surface density profile (Tables 6 and 7), because of the central ($\tilde{r} \lesssim 0.2$) deficit of SNe. However, in the $\tilde{r} \in [0.2; \infty)$ range, the inconsistency vanishes for CC SNe in most of the subsamples of spiral galaxies. In the inner-truncated disc, only the radial distribution of CC SNe in barred early-type spirals is inconsistent with an exponential surface density profile, which appears to be caused by the impact of bars on the radial distribution of CC SNe.

(vi) In the inner regions of non-disturbed spiral hosts, we do not detect a relative deficiency of Type Ia SNe with respect to CC (Table 5), contrary to what was found by other authors, who had explained this by possibly stronger dust extinction for Type Ia than for CC SNe. Instead, the radial distributions of both types of SNe are similar in all the subsamples of Sa–Sbc and Sc–Sm galaxies (Table 4), which supports the idea that the relative increase of CC SNe in the inner regions of spirals found by the other authors is most probably due to the central excess of CC SNe in disturbed galaxies.

(vii) As was found in earlier studies, the physical explanation for the more concentrated distribution of SNe Ibc with respect to SNe II in non-disturbed and unbarred spiral galaxies (Fig. 3) is that SNe Ibc arise from more metal-rich environments. The radial distributions of Types Ib and Ic SNe are sufficiently similar that the KS and AD tests fail to distinguish them with statistical significance.

ACKNOWLEDGEMENTS

We would like to thank the anonymous referee for his/her excellent commentary, and also V. de Lapparent, E. Bertin, and T.A. Nazaryan for their constructive comments on the earlier drafts of this manuscript. AAH, AGK, LVB, and ARP acknowledge the hospitality of the Institut d'Astrophysique de Paris (France) during their stay as visiting scientists supported by the Programme Visiteurs Extérieurs (PVE). This work was supported by State Committee Science MES RA, in frame of the research project number SCS 13–1C013. AAH is also partially supported by the ICTP. VA is supported by grant SFRH/BPD/70574/2010 from FCT (Portugal). DK acknowledges financial support from the Centre National d'Études Spatiales (CNES). MT is partially supported by the PRIN-INAF 2011 with the project Transient Universe: from ESO Large to PESSTO. This work was made possible in part by a research grant from the Armenian National Science and Education Fund (ANSEF) based in New York, USA. Funding for SDSS-III has been provided by the Alfred P. Sloan Foundation, the Participating Institutions, the National Science Foundation, and the US Department of Energy Office of Science. The SDSS–III web site is http://www.sdss3.org/. SDSS–III is managed by the Astrophysical Research Consortium for the Participating Institutions of the SDSS–III Collaboration including the University of Arizona, the Brazilian Participation Group, Brookhaven National Laboratory, University of Cambridge, University of Florida, the French Participation Group, the German Participation Group, the Instituto de Astrofisica de Canarias, the Michigan State/Notre Dame/JINA Participation Group, Johns Hopkins University, Lawrence Berkeley National Laboratory, Max Planck Institute for Astrophysics, New Mexico State University, New York University, Ohio State University, Pennsylvania State University, University of Portsmouth, Princeton University, the Spanish Participation Group, University of Tokyo, University of Utah, Vanderbilt University, University of Virginia, University of Washington, and Yale University.

REFERENCES

Ahn C. P., et al., 2014, ApJS, 211, 17
Anderson J. P., James P. A., 2009, MNRAS, 399, 559
Anderson J. P., Habergham S. M., James P. A., Hamuy M., 2012, MNRAS, 424, 1372
Anderson J. P., James P. A., Habergham S. M., Galbany L., Kuncarayakti H., 2015a, PASA, 32, 19
Anderson J. P., James P. A., Förster F., González-Gaitán S., Habergham S. M., Hamuy M., Lyman J. D., 2015b, MNRAS, 448, 732
Baillard A., et al., 2011, A&A, 532, A74
Barbon R., Capaccioli M., Ciatti F., 1975, A&A, 44, 267
Barbon R., Buondí V., Cappellaro E., Turatto M., 1999, A&AS, 139, 531
Barnard G. A., 1945, Nature, 156, 177
Bartunov O. S., Tsvetkov D. I., 1986, Ap&SS, 122, 343
Bartunov O. S., Makarova I. N., Tsvetkov D. I., 1992, A&A, 264, 428
Bartunov O. S., Tsvetkov D. Y., Filimonova I. V., 1994, PASP, 106, 1276
Bernardi M., Meert A., Vikram V., Huertas-Company M., Mei S., Shankar F., Sheth R. K., 2014, MNRAS, 443, 874
Boissier S., Prantzos N., 2009, A&A, 503, 137
Bressan A., Della Valle M., Marziani P., 2002, MNRAS, 331, L25
Cameron E., 2011, PASA, 28, 128
Cappellaro E., Turatto M., Tsvetkov D. Y., Bartunov O. S., Pollas C., Evans R., Hamuy M., 1997, A&A, 322, 431
D'Agostino R. B., Stephens M. A., 1986, Goodness-of-fit techniques
Engmann S., Cousineau D., 2011, J. Appl. Quant. Methods, 6, 1
Filippenko A. V., 1997, ARA&A, 35, 309
Gadotti D. A., 2009, in Contopoulos G., Patsis P., eds, Barred Galaxies: an Observer's Perspective, Springer, Berlin. p. 159
Galbany L., et al., 2014, A&A, 572, A38
Habergham S. M., James P. A., Anderson J. P., 2012, MNRAS, 424, 2841
Habergham S. M., Anderson J. P., James P. A., Lyman J. D., 2014, MNRAS, 441, 2230
Hakobyan A. A., 2008, Astrophysics, 51, 69
Hakobyan A. A., Petrosian A. R., McLean B., Kunth D., Allen R. J., Turatto M., Barbon R., 2008, A&A, 488, 523
Hakobyan A. A., Mamon G. A., Petrosian A. R., Kunth D., Turatto M., 2009, A&A, 508, 1259 (H09)
Hakobyan A. A., et al., 2011, Astrophysics, 54, 301
Hakobyan A. A., Adibekyan V. Z., Aramyan L. S., Petrosian A. R., Gomes J. M., Mamon G. A., Kunth D., Turatto M., 2012, A&A, 544, A81 (Paper I)
Hakobyan A. A., et al., 2014, MNRAS, 444, 2428 (Paper II)
Hamuy M., Pinto P. A., 1999, AJ, 117, 1185
Hatano K., Branch D., Deaton J., 1998, ApJ, 502, 177
Herrero-Illana R., Pérez-Torres M. Á., Alberdi A., 2012, A&A, 540, L5
Holwerda B. W., Reynolds A., Smith M., Kraan-Korteweg R. C., 2015, MNRAS, 446, 3768
Howell D. A., Wang L., Wheeler J. C., 2000, ApJ, 530, 166
Ivanov V. D., Hamuy M., Pinto P. A., 2000, ApJ, 542, 588
Iye M., Kodaira K., 1975, PASJ, 27, 411
James P. A., Anderson J. P., 2006, A&A, 453, 57
James P. A., Percival S. M., 2015, MNRAS, 450, 3503
James P. A., Bretherton C. F., Knapen J. H., 2009, A&A, 501, 207
Johnson H. M., MacLeod J. M., 1963, PASP, 75, 123
Kangas T., Mattila S., Kankare E., Kotilainen J. K., Väisänen P., Greimel R., Takalo A., 2013, MNRAS, 436, 3464
Kazarian M. A., 1997, Astrophysics, 40, 296
Kormendy J., Kennicutt Jr. R. C., 2004, ARA&A, 42, 603

Leaman J., Li W., Chornock R., Filippenko A. V., 2011, MNRAS, 412, 1419
Li W., Li Z., 1995, A&A, 301, 666
Li W., Chornock R., Leaman J., Filippenko A. V., Poznanski D., Wang X., Ganeshalingam M., Mannucci F., 2011, MNRAS, 412, 1473
Mannucci F., Della Valle M., Panagia N., Cappellaro E., Cresci G., Maiolino R., Petrosian A., Turatto M., 2005, A&A, 433, 807
Maoz D., Mannucci F., Nelemans G., 2014, ARA&A, 52, 107
Massey F. J., 1951, J. Am. Stat. Assoc., 46, 68
McCarthy M. F., 1973, Ric. Astron., 8, 411
McMillan R. J., Ciardullo R., 1996, ApJ, 473, 707
Navasardyan H., Petrosian A. R., Turatto M., Cappellaro E., Boulesteix J., 2001, MNRAS, 328, 1181
Nazaryan T. A., Petrosian A. R., Hakobyan A. A., Adibekyan V. Z., Kunth D., Mamon G. A., Turatto M., Aramyan L. S., 2013, Ap&SS, 347, 365
Onic D., Arbutina B., Urosevic D., 2008, Rev. Mex. Astron. Astrofis., 44, 103
Oohama N., Okamura S., Fukugita M., Yasuda N., Nakamura O., 2009, ApJ, 705, 245
Petrosian A. R., Turatto M., 1990, A&A, 239, 63
Petrosian A. R., Turatto M., 1995, A&A, 297, 49
Petrosian A., et al., 2005, AJ, 129, 1369
Pettitt A. N., 1976, Biometrika, 63, 161
Prieto J. L., Stanek K. Z., Beacom J. F., 2008, ApJ, 673, 999
Shaw R. L., 1979, A&A, 76, 188
Simien F., de Vaucouleurs G., 1986, ApJ, 302, 564
Smartt S. J., 2009, ARA&A, 47, 63
Smith N., Li W., Filippenko A. V., Chornock R., 2011, MNRAS, 412, 1522
Spergel D. N., et al., 2007, ApJS, 170, 377
Stanishev V., Rodrigues M., Mourão A., Flores H., 2012, A&A, 545, A58
Tsvetkov D. Y., 1981, Sov. Astron. Lett., 7, 254
Tsvetkov D. Y., 1987, Sov. Astron., 31, 39
Tsvetkov D. Y., Pavlyuk N. N., Bartunov O. S., 2004, Astron. Lett., 30, 729
Turatto M., 2003, in Weiler K., ed., Lecture Notes in Physics, Vol. 598, Supernovae and Gamma-Ray Bursters, Springer-Verlag, Berlin. p. 21
Turatto M., Cappellaro E., Petrosian A. R., 1989, A&A, 217, 79
Vettolani G., Zamorani G., 1977, MNRAS, 178, 693
Wang L., Höflich P., Wheeler J. C., 1997, ApJ, 483, L29
Wang J., Deng J. S., Wei J. Y., 2010, MNRAS, 405, 2529
Wang X., Wang L., Filippenko A. V., Zhang T., Zhao X., 2013, Science, 340, 170
Yoshizawa M., Wakamatsu K., 1975, A&A, 44, 363
de Lapparent V., Baillard A., Bertin E., 2011, A&A, 532, A75
van den Bergh S., 1997, AJ, 113, 197
van den Bergh S., McClure R. D., 1990, ApJ, 359, 277

SUPPORTING INFORMATION

Additional Supporting Information may be found in the online version of this article:

PaperIIIonlinedata.csv
(http://www.mnras.oxfordjournals.org/lookup/suppl/doi:10.1093/mnras/stv2853/-/DC1).

Please note: Oxford University Press is not responsible for the content or functionality of any supporting materials supplied by the authors. Any queries (other than missing material) should be directed to the corresponding author for the article.